Pure exciton- and magnon-assisted optical transitions in the one-dimensional antiferromagnet $CsMnCl_3 \cdot 2H_2O$ (CMC)

Weiyi Jia,* E. Strauss,† and W. M. Yen
Department of Physics, University of Wisconsin, Madison, Wisconsin 53706
(Received 26 January 1981)

We report the first observation of the pure electronic transitions in the $^4T_1$ state of Mn^{2+} ions in the one-dimenisional antiferromagnet $CsMnCl_3 \cdot 2H_2O$ (CMC) in the absorption, excitation, and fluorescence spectra. Selection rules are analyzed: the exciton transition is electric dipole allowed, the magnon sideband in emission is a single-ion process, and is both electric and magnetic dipole allowed; however, the magnon sideband in absorption is an ion-pair process and is a weakened-electric-dipole and magnetic-dipole transition. The density of magnon states and the line profile of the magnon sideband have been calculated. The results explain the peculiar line shapes of the observed sideband emission. An exponential decay of the exciton is observed with a lifetime of 0.57 ms.

I. INTRODUCTION

The properties of one-dimensional magnetic materials have been of some current interest, with the optical properties being no exception. A number of studies have appeared recently which indicate that the optical excitation is localized in various quasi-one-dimensional compounds such as $(CH_3)_4NMnCl_3$ (TMMC),[1] $CsMnBr_3$,[2] and $CsMnCl_3 \cdot 2H_2O$ (CMC).[3] Because of this localization and the macroscopic dynamics of trapping in low-dimensionality systems at low temperatures, the lifetimes and emission from the optically excited state is much less sensitive to the presence of irregular or impurity sites, as in the case, for example, in MnF_2, thus the intrinsic properties of Mn^{2+} excitations in these systems may, one hopes, be derived directly from such emission studies.

Most of the work carried out to date has been done on the phonon-assisted or phonon sidebands of the $^4T_1$ state of Mn^{2+}. This is because the pure electronic transitions from and to the ground state $^6A_1$ are generally very weak due to selection rules. Recently, however, Bron and his co-workers[3] have reported the presence of weak fine structure adjacent to the $^4T_1$ phonon sideband of CMC both in excitation (absorption) and emission spectra. They designated this structure as the pure exciton transition but they failed to explain why the positions of the excitonic transitions in absorption and fluorescence differed in energy by some 21 cm^{-1}, configurational shifts being very rare in this Mn^{2+} state.

In this paper, we report on a laser based optical study of CMC at low temperatures in which we have been able to observe and identify the no-magnon, no-phonon $^4T_1$ pure electronic transition of Mn^{2+}. The fine structure observed in emission by the Russian workers has been reconfirmed in our study but it is now identifiable as the magnon sidebands of the pure excitons thus explaining the energy shift in absorption and emission alluded to above. We also present here a discussion on the optical selection rules and transition mechanism for the exciton and exciton-magnon assisted transition as well as a calculation of the magnon density of states and the magnon sideband shapes. The decay processes affecting the exciton and magnon systems have also been measured and reported below.

II. EXPERIMENTAL DETAILS

CMC is a well-known quasi-one-dimensional antiferromagnetic (AF) Mn^{2+} compound. It has an orthorhombic structure with a space group $P_{cca} - D_{2h}^8$.[4] It orders magnetically into space group $P_{2bc'ac'}$ (Ref. 5) with a Néel temperature, $T_N = 4.89$ K. The chemical unit cell contains four formula units and has dimensions $a = 9.060$ Å, $b = 7.285$ Å, and $c = 11.455$ Å (Fig. 1). The magnetic unit cell consists of two such chemical cells combined along the b axis, resulting in eight Mn^{2+} ions in each magnetic unit cell.

The strongest exchange interactions occur along with Mn–Cl–Mn–Cl linear chains parallel to the a axis.[6] Interchain exchange interactions are generally very weak because of the intervening of at least two nonmagnetic ions. At temperatures $T < T_N$, these latter interactions cause a three-dimensional long-range order.

The local site symmetry of Mn^{2+} ions is C_2. Each Mn^{2+} ion is surrounded by a highly distorted oc-

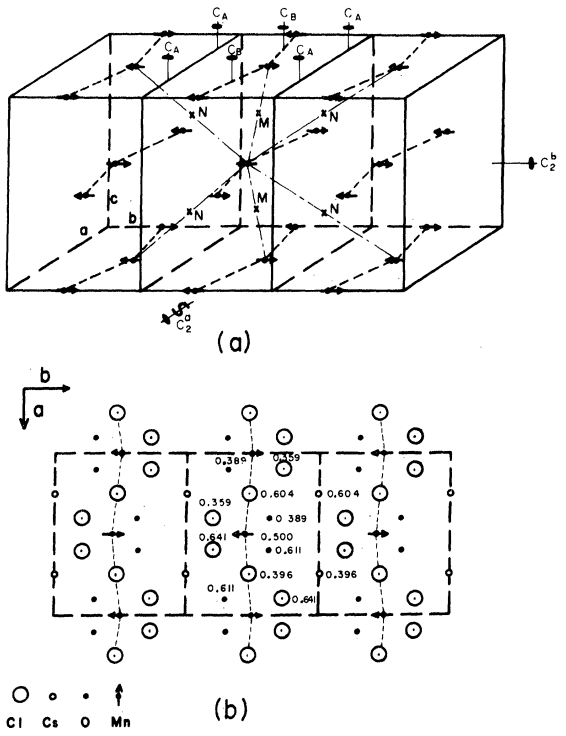

FIG. 1. (a) The distribution of the Mn^{2+} ions in the unit cells of CMC and the positions of some symmetry axes and inversion centers. For convenience, here the unit cells are shifted along the z axis from the ordinary crystallographic cell by $z=-0.25$. There are three such chemical units combined along the b axis. The magnetic cell consists of two adjacent chemical cells. (b) A (001) projection of the mediate part of these three unit cells, the Mn^{2+} ions are at $z=0.5$.

tahedron consisting of four chlorine and two oxygens (Fig. 1). Thus the Mn sites do not possess inversion symmetry and electric dipole transitions are possible.

$CsMnCl_3 \cdot 2H_2O$ single crystals were grown from the supersaturated solutions with $CsCl:MnCl_2 \cdot 4H_2O = 1:1$ by evaporation of water. The growing temperature was maintained at 35 °C. The raw materials used had quoted purities of (99.9% CsCl, 99% $MnCl_2 \cdot 4H_2O$) and (99.999 CsCl, 99.99% $MnCl_2 \cdot 4H_2O$). Most of the data in this work were taken from higher purity crystals, though it was found that the optical properties do not depend greatly on the impurity content of the constituents.

A combination of optical techniques were used in this study. Conventional methods were used to obtain the absorption spectra. The fluorescence spectra were obtained by using the 5145-Å line of a cw argon laser (~500 mW) or the second harmonic (5320 Å) of a Nd:YAG (yttrium aluminum garnet) pulsed laser ($\sim \frac{1}{2}$ MW) to pump the $^4T_1$ phonon sideband. For the excitation spectra we utilized a grazing incidence tunable dye laser pumped by either the YAG laser or a N_2 laser; the pulsed nature of these latter sources also allowed us to measure the various decay times. Various spectrometers with typical resolutions of ~1 cm^{-1} were used to analyze the signals; standard Hg spectra were used to calibrate line positions. A RCA 31034A tube was used to detect the signal and photon counting techniques were employed whenever necessary.

To achieve low temperatures, the samples were immersed in superfluid helium (1.8–2.0 K). For temperatures $T > 2$ K the samples were cooled by a Heli-tran cryostat.

III. EXPERIMENTAL RESULTS

The low-temperature (1.8 K) absorption spectrum of CMC in the 5400-Å region is shown in Fig. 2; the spectrum is dominated by a broad band peaking at 5390 Å which is phonon assisted. Some weak structure can be observed in the absorption trace. Following the identification of the pure electronic transition (to be discussed below), this structure is likely a vibrational progression of phonon modes and will not be emphasized here. Germane to this work is the fine structure appearing at the low-energy side of the absorption trace, which is expanded in the inset. A weak and sharp absorption located at 17 064.0 cm^{-1} (5860.3 Å) is accompanied by a broad shoulder to the high-energy side. The absorption coefficients for these two features are approximately 0.009 and 0.004 cm^{-1}, respectively, and they are not observed by conventional spectroscopic means unless large crystalline samples are used. The traces shown in Fig. 2 were obtained in a 8-mm-thick sample.

We believe that the sharp transition is one of the unassisted $^4T_1$ pure exciton states of Mn^{2+} in CMC, while the broad feature is the magnon sideband of

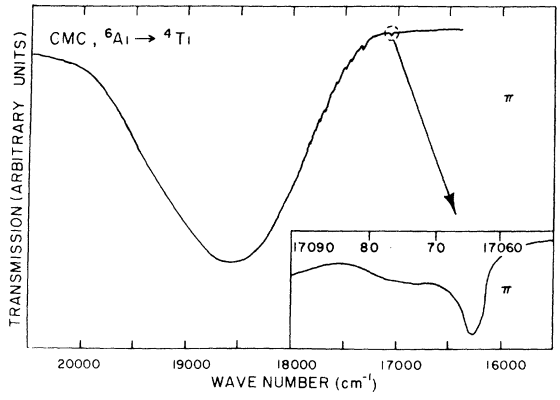

FIG. 2. The $^4T_1$ phonon sideband and the pure exciton line (enlarged in the inset) in the π-polarization absorption spectrum of CMC at 2 K.

this transition.

In view of the weakness of the absorption and in order to obtain confirmation of our assignment, we conducted time-resolved spectroscopy using a high-power tunable laser. By gating the detection system close to the pulse excitation, thus preempting excitation transfer, and by monitoring the stronger phonon sideband emission, the excitation spectrum is complementary to the absorption spectrum. Results are shown in Fig. 3(a) for $T=1.8$ K and for three different polarizations. We note that the general features are the same as that shown for the absorption in the inset of Fig. 2. However, the σ and α active spectra are identical, whereas the π-polarized spectrum has an additional shoulder on the low-energy side which is only barely discernible in the absorption trace. The similarity between σ and α indicates that these transitions are electric dipole active.

We have also investigated the emission spectra of CMC at low temperatures. Again as is usual in Mn^{2+} compounds a broad, strong phonon assisted emission peaking at 6425 Å is observed. On the high-energy side of the emission fine structure again appears at low temperatures ($T<10$ K) which consists of a sharp transition accompanied by broader structure. The emission spectra in this region are shown in Fig. 3(b). We note that the sharp line in emission is located at 5860.2 Å (17064.3 cm^{-1}) and that this is in coincidence with the position of the exciton transition in absorption or excitation. It is likely that Bron *et al.* mistook the broader structure in emission, i.e., the sideband, as the origin of the emission. It is also evident from Fig. 3(b) that the σ and α polarized are again identical with each other and that shoulderlike structure appears on the high-energy side of the no-phonon, no-magnon transition in these polarizations. The π-polarized spectrum, on the other hand, is relatively simple in this case; the inhomogeneous linewidth of the pure electronic transition is 4.3 cm^{-1}.

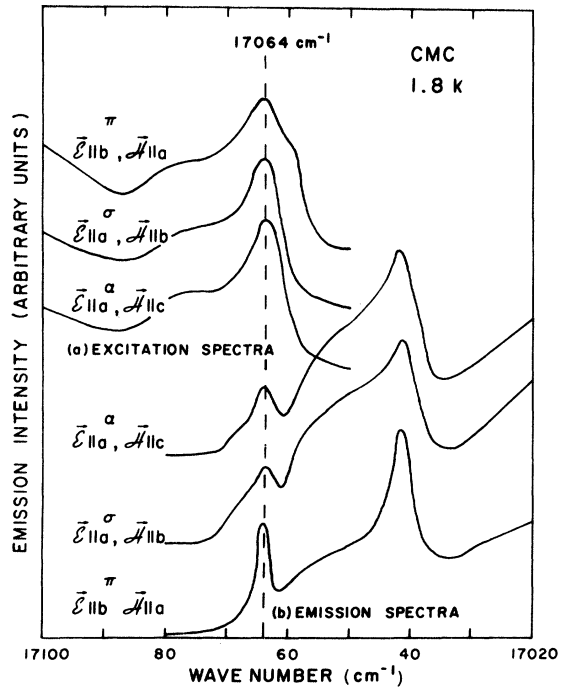

FIG. 3. The excitons and the magnon sidebands in excitation and emission spectra of CMC at 1.8 K.

In the above configuration of polarizations, we defined π polarization as $\vec{\mathcal{E}}\|b$ and $\vec{\mathcal{H}}\|a$, σ as $\vec{\mathcal{E}}\|a$ and $\vec{\mathcal{H}}\|b$, and α as $\vec{\mathcal{E}}\|a$ and $\vec{\mathcal{H}}\|c$. Here $\vec{\mathcal{E}}$ and $\vec{\mathcal{H}}$ are the electric and magnetic field of the light. However, we note that for the orthorhombic crystal, there are two nonequivalent configurations for each polarization. For example, we can define σ' as $\vec{\mathcal{E}}\|c$ and $\vec{\mathcal{H}}\|b$, and α' as $\vec{\mathcal{E}}\|c$ and $\vec{\mathcal{H}}\|a$. In order to see the difference between them, we measured the σ'-polarization absorption and emission spectra, the results are shown in Figs. 4(a) and 4(b). Similar results for the α' polarization were obtained. It can be seen from Figs. 3(a) and 3(b) and Figs. 4(a) and 4(b) that the difference between the σ' and σ polarization spectrum is very obvious. There appears a second peak between the exciton and the shoulder in the absorption, and the shoulder in emission goes up and becomes stronger.

Both the exciton and magnon sideband become broader as the temperature is increased. Analysis of temperature effects is made difficult because of a concomitant thermal broadening and interference from the phonon sidebands; nevertheless, the exciton and its magnon sideband persist well above T_N. Figure 5 shows the fine structure in emission in such case ($T=5.5$ K).

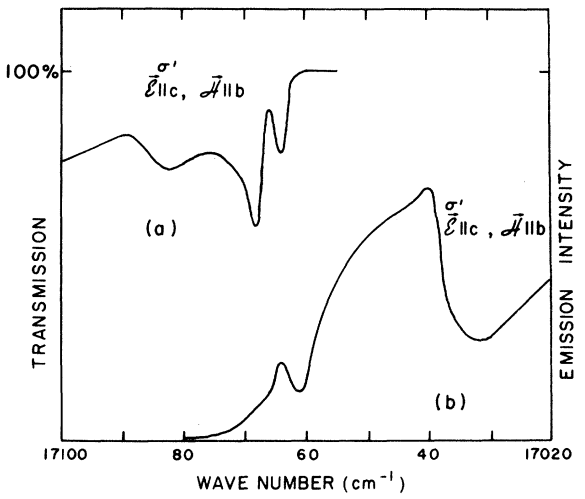

FIG. 4. The exciton and the magnon sidebands in the σ'-polarization absorption (a) and emission (b) spectra of CMC at 1.8 K.

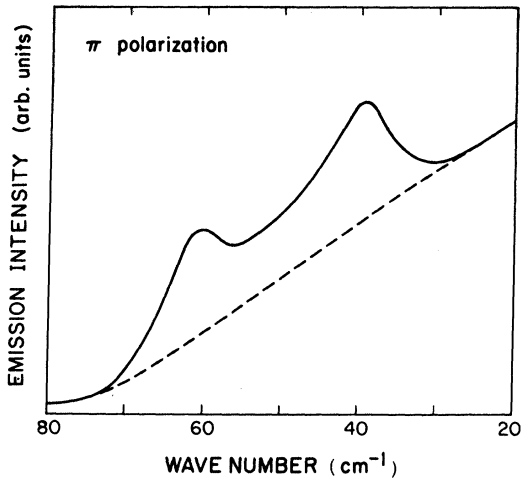

FIG. 5. The exciton and the magnon sideband in the emission spectrum above the Néel temperature. $T=5.5$ K. The origin of the abscissa is at 17 080 cm^{-1}.

The emission from the $^4T_1$ state of CMC shows a lifetime of 0.57 ms that is typically exponential over several decades (Fig. 6). This is so whether the exciton, the magnon sideband, or the phonon sideband emission is monitored. This behavior attests to the reduced importance of trapping in irregular sites for low-dimensionality systems. The lifetime shows a very weak dependence on increased temperature ($\tau=0.54$ ms at $T=5.5$ K) again, we believe, a consequence of the dimensionality.

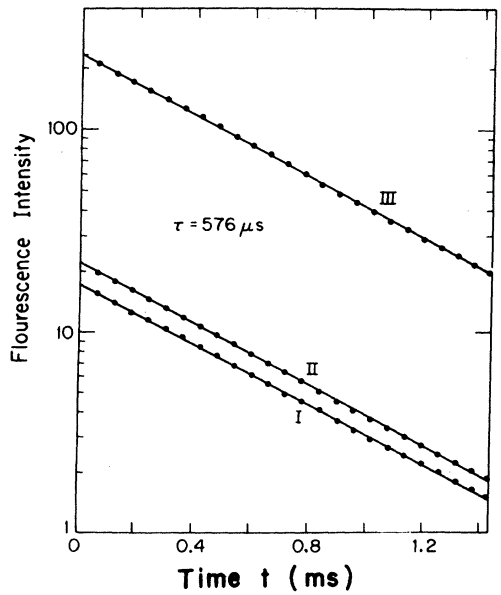

FIG. 6. The decay curves of the exciton (I), the magnon sideband (II), and the phonon sideband (III) of CMC at 1.8 K.

IV. THEORETICAL CONSIDERATIONS

A. Selection rules

We have noted earlier that the Mn^{2+} ion sites are located at the center of a highly distorted octahedron and have no inversion symmetry. Because of this, we might expect that the $^6A_1 \rightarrow {}^4T_1$ pure electronic transitions will be electric dipole allowed through a higher-order mechanism which admixes odd parity into the $^4T_1$ wave functions. At the same time, the spin selection rule is relaxed by the spin-orbit coupling between the ground and excited states, as in MnF_2.[7] That these expectations are correct can be seen from both Figs. 3(a) and 3(b), where as we have also noted the σ- and α-polarized spectra of the pure exciton transition are identical, differing from the π spectra in each case.

The magnon sideband in absorption which appears as a shoulder or a weak peak adjacent to the excitonic transition at the high-energy side is generally accepted to be an ion pair process[7–9] occurring in ions in two different sublattices [Fig. 7(a)]. In the case of MnF_2 where the Mn^{2+} ions at ground states are at inversion symmetry centers, a Tanabe-Moriya-Sugano ion pair,[8] in which one is in a magnon state and its nearest neighbor is in an excitonic state, however, contains an odd parity component in the $^4T_1$ excitonic state wave function. In the case of CMC, it seems that the odd parity component from the combination of such Tanabe-Moriya-Sugano ion pairs and original odd parity component of $^4T_1$ wave function coming from the noninversion symmetry tends to partly compensate each other. Consequently the electric

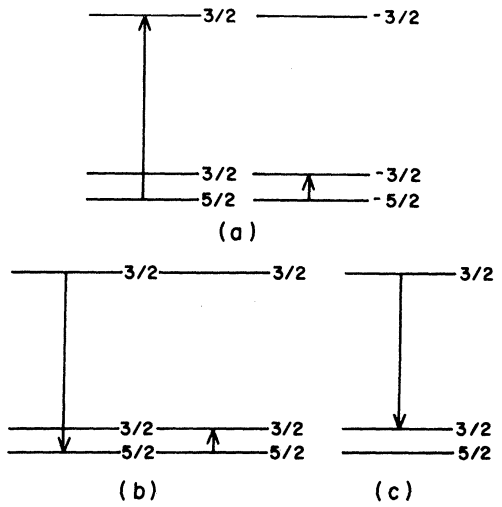

FIG. 7. (a) The ion-pair process in absorption; (b) the ion-pair process in emission; and (c) the single-ion process in emission.

dipole-allowed transition is weakened and its contribution to the magnon sideband is of the same order as that of a magnetic dipole transition, thus the magnon sideband becomes a weak shoulder, as shown in Fig. 3(a). An exception is the secondary magnon peak, shown in Fig. 4(a), which will be discussed later.

For the emission spectrum, there are two possible processes, as are illustrated in Figs. 7(b) and 7(c). One occurs between pairs of ions in the same sublattice, another at a single-ion site, which is a single-ion process. Following the same argument for the absorption spectrum, the ion pair process would be very weak. The single ion process is both electric and magnetic dipole allowed. Therefore, in the emission spectrum, we expect a stronger magnon sideband [Fig. 3(b)].

We can directly write the transition matrix element for the single-ion process

$$M_k = \vec{\mathcal{E}} \cdot \langle M, \vec{k} | \vec{p} | E, \vec{k} \rangle \ . \tag{1}$$

Here $\vec{p}$ is an electric dipole operator, $\vec{\mathcal{E}}$ is an optical electric field, $|E, \vec{k}\rangle$ and $\langle M, \vec{k}|$ are the exciton and magnon wave function with the wave vector $\vec{k}$, respectively. Both of them are not single energy levels, but energy bands. For the A-sublattice magnon, we have[7]

$$|M^A\rangle = N^{-1/2} \sum_n e^{-i\vec{k}\cdot\vec{r}_{An}} |M_{An}\rangle \ . \tag{2}$$

The dispersion of the exciton is generally small, so we can take it as a single-ion level described by $|E\rangle$. For the magnon wave function of a single ion, we might approximate it as the sum of neighbor's contributions with different phase factors, in spite of the fact that the magnons are cooperative and spread throughout the lattice. As a result, we can formally get the same expressions for the matrix elements between the same sublattice ions and between the different sublattice ions, respectively, as in the pair process.[7]

$$M_k = \sum_n e^{i\vec{k}\cdot\vec{r}_{An}} \vec{\mathcal{E}} \cdot \langle M_{An} | \vec{p} | E_A \rangle \ , \tag{3}$$

$$N_k = \sum_m e^{i\vec{k}\cdot\vec{r}_{Bm}} \vec{\mathcal{E}} \cdot \langle M_{Bm} | \vec{p} | E_A \rangle \ . \tag{4}$$

The summations are over the next-nearest neighbors in the same sublattice and over the nearest neighbors in the opposite sublattice, respectively. It will be seen later that, for the emission, the contribution of N_k from the opposite sublattice ions actually vanishes near the Brillouin-zone boundary.

B. Magnon properties in CMC

We consider next the magnon dispersion relation and the magnon density of states in CMC. We make the simplifying approximation that CMC may be treated as a simple two sublattice antiferromagnet, in spite of the fact that the primitive magnetic cell is complex and the Mn–Cl–Mn chains along the a axis have a slight zig-zag structure.

The dispersion relation for the magnons may be written as

$$E_m(k) = [(A - I_k)^2 - J_k^2]^{1/2} \ , \tag{5}$$

where

$$A = g\mu H_a - 4S(J_1 + J_2 + J_3) + 16S(J_4 + J_5 + J_6) \ , \tag{6}$$

$$I_k = 16S(J_4 \cos\tfrac{1}{2}k_a a \cos k_b b + J_5 \cos k_b b \cos\tfrac{1}{2}k_c c + J_6 \cos\tfrac{1}{2}k_c c \cos\tfrac{1}{2}k_a a) \ , \tag{7}$$

$$J_k = 4S(J_1 \cos\tfrac{1}{2}k_a a + J_2 \cos k_b b + J_3 \cos\tfrac{1}{2}k_c c) \ , \tag{8}$$

in the above $J_{1,2,3}$ are nearest-neighbor exchange integrals along the a, b, and c axes, respectively, and are negative (antiferromagnetic coupling). $J_{4,5,6}$ are exchange integrals between next-nearest neighbors in the ab, bc, and ca planes, respectively; these integrals are positive. H_a is the anisotropic field. Using values from Ref. 6, $J_1 = -2.48$ cm^{-1}, $J_2 + J_3 = -0.017$ cm^{-1}, and $g\mu H_a = 0.024$ cm^{-1}. No experimental data exist for $J_{4,5,6}$ but they are presumably very small positive numbers which we will assume to be zero. The maximum magnon energy at the Brillouin-zone (BZ) boundary is then from Eq. (5),

$$E_{\max} = 25.0 \text{ cm}^{-1} \ .$$

The density of magnon states with energy E is defined as

$$\rho(E) = \sum_k^{\text{BZ}} \delta(E - E_m(k)) \ . \tag{9}$$

The summation is over the entire Brillouin zone (BZ). The results of the calculation are shown in Fig. 8 for CMC. We note that there is a density peak near the origin corresponding to points

$$Y(k_a = 0, k_c = 0, k_b = \pi/2b) \ ,$$

$$Z(k_a = 0, k_b = 0, k_c = \pi/c) \ ,$$

and

$$T(k_a = 0, k_b = \frac{\pi}{2b}, k_c = \pi/c) \ ,$$

of the BZ. We also note that the density is considerable in all regions connecting these points to the R, S, U, and X symmetry points of the BZ (see Fig. 8). We will show in the next section that this gives

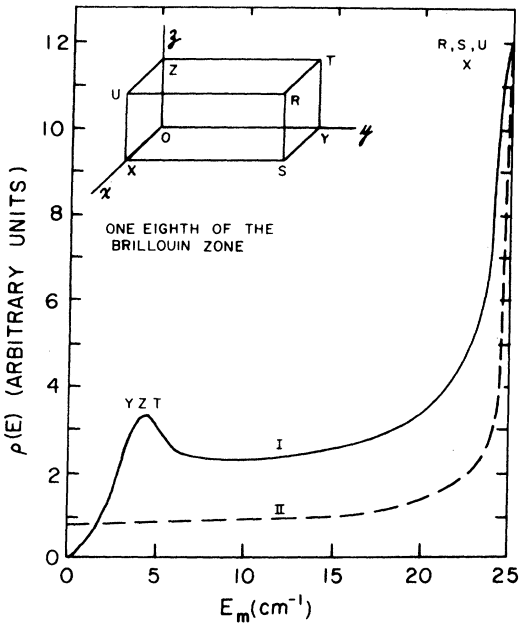

FIG. 8. The density of the magnon states for CMC. I, the three-dimensional case; II, the one-dimensional approximation. The inset is one-eighth of the Brillouin zone.

rise to the peculiar profiles of the magnon sidebands. This type of density function is to be expected in any quasi-one-dimensional magnetic system with linear chain exchange interactions and low magnetic anisotropy when the system orders in three dimensions.

Finally, if we assume that CMC is an ideal one-dimensional system Eqs. (5) and (10) reduce to

$$E_m'(k) = |4SJ_1| \sin \tfrac{1}{2} k_a a \tag{10}$$

$$\rho'(E) = \sum_{k=0}^{\pi} \delta(E - |4SJ_1| \sin \tfrac{1}{2} k)$$

$$= \int_o^{\pi} \delta(E - |4SJ_1| \sin \tfrac{1}{2} k)\, dk$$

$$= 2[(4SJ_1)^2 - E^2]^{-1/2} \ . \tag{11}$$

Here $k = k_a a$ and $0 \leq E \leq 4SJ_1$. The density function, Eq. (11), is also shown in Fig. 8 and it differs from the three-dimensional case considerably. We again shall see that the line shape of the magnon sideband in CMC cannot be explained under the one-dimensional simplification.

C. Line shape of the magnon sidebands

Because magnon-exciton interaction effects are minimized in the emission spectra,[10] we initially focus our attention on these processes. From Fig. 3(b), we note that the exciton-magnon sideband splitting is 22.8 cm^{-1} compared to the calculated value of 25.0 cm^{-1}. The small discrepancy may be attributed to our simplifying assumptions in Eq. (5) and/or to a small dispersion of the exciton. The latter is also consistent with values obtained for the $^4T_1$ exciton in other Mn^{2+} compounds.[11]

In the zero temperature approximation, the transition intensity of magnon sidebands in emission may be written[12]

$$E(\omega) = C \sum_{k}^{BZ} (|M_k|^2 U_k^2 + |N_k|^2 V_k^2) \times \delta(\hbar\omega - E_0 + E_m(k)) \ . \tag{12}$$

We are neglecting in Eq. (12) as is customary the excitonic inter- and intra-sublattice transfer terms that lead to E_0 dispersion, C is a constant, M_k and N_k are given in Eqs. (3) and (4), and U_k^2 and V_k^2 are the canonical transformation coefficients of the magnon operators and are plotted in Fig. 9 for CMC. Near the BZ boundary, $V_k^2 \simeq 0$, so that the $|N_k|^2$ contribution vanishes at these points as we have noted in Sec. IV A.

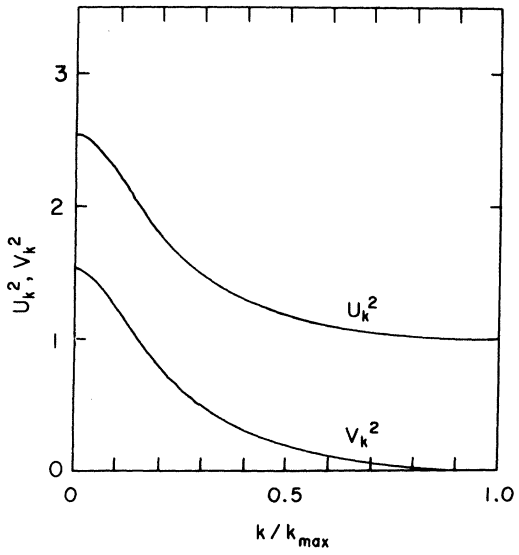

FIG. 9. Variation of U_k^2 and V_k^2 in CMC as function of k along the a axis.

CMC has low symmetry (Fig. 1 and Appendix A) and the magnetic cell structure is very complex. In order to keep the adjustable parameters to as few as possible, we make a number of necessary approximations. In the calculation, in some cases we consider only the symmetry of the Mn^{2+} distributions and ignore the zig-zag structure of the linear chains. We also assume that the exchange elements of the four next-nearest neighbors in the *ab* or *bc* or *ac* plane to the central ion have the same absolute values. Under these conditions, the transition intensity can be obtained:

$$E^{\pi}=A_4^2\sum_k^{BZ}\sin^2\tfrac{1}{2}k_a a\sin^2 k_b b U_k^2\delta(\hbar\omega-E_0+E_m(k))+\sum_k^{BZ}(B_2\sin k_b b+B_3\sin\tfrac{1}{2}k_c c)^2V_k^2\delta(\hbar\omega-E_0+E_m(k)) \tag{13}$$

for the π-polarization ($\vec{\mathcal{E}}||b$),

$$E^{\sigma}=\sum_k^{BZ}(C_4\cos\tfrac{1}{2}k_a a\cos k_b b+C_6\sin\tfrac{1}{2}k_a a\sin\tfrac{1}{2}k_c c)^2U_k^2\delta(\hbar\omega-E_0+E_m(k))$$
$$+\sum_k^{BZ}(D_2^2\sin^2 k_b b+D_3^2\cos^2\tfrac{1}{2}k_c c)V_k^2\delta(\hbar\omega-E_0+E_m(k)) \tag{14}$$

for the σ-polarization ($\vec{\mathcal{E}}||a$), and

$$E^{\sigma'}=F_6^2\sum_k^{BZ}\sin^2\tfrac{1}{2}k_a a\sin^2\tfrac{1}{2}k_c c U_k^2\delta(\hbar\omega-E_0+E_m(k))$$
$$+\sum_k^{BZ}(G_1\cos\tfrac{1}{2}k_a a+G_3\cos\tfrac{1}{2}k_c c)^2V_k^2\delta(\hbar\omega-E_0+E_m(k))+G_2^2\sum_k^{BZ}\sin^2 k_b b V_k^2\delta(\hbar\omega-E_0+E_m(k)) \tag{15}$$

for the σ' polarization ($\vec{\mathcal{E}}||c$).

For the absorption transition similar expressions can be obtained by exchanging U_k^2 and V_k^2 and replacing the positive sign before $E_m(k)$ with the negative sign. For example, for the σ'-polarization absorption transition,

$$A^{\sigma'}=\sum_k^{BZ}(G_1\cos\tfrac{1}{2}k_a a+G_3\cos\tfrac{1}{2}k_c c)^2U_k^2\delta(\hbar\omega-E_0-E_m^a(k))$$
$$+G_2^2\sum_k^{BZ}\sin^2 k_b b U_k^2\delta(\hbar\omega-E_0-E_m^a(k))+F_6^2\sum_k^{BZ}\sin^2\tfrac{1}{2}k_a a\sin^2\tfrac{1}{2}k_c c V_k^2\delta(\hbar\omega-E_0-E_m^a(k)) \ . \tag{16}$$

In Eqs. (13)–(16), the subscripts $1,2,3,\ldots,6$ of the constants $A_2,B_2,B_5,\ldots,F_6$ correspond to the subscripts $1,2,3,\ldots,6$ of $J_{1,2,3,\ldots,6}$, respectively, and they indicate with which neighbor of the center ion these constants are related. Note that only $E^{\sigma'}$ and $A^{\sigma'}$ include the term G_1 which is related with the strongest interaction of the chain *a*. $E_m^a(k)$ in Eq. (16) indicates a modified magnon dispersion, see Eqs. (17)–(19) below.

Figure 10 shows the observed and calculated line profiles of the magnon sideband in emission for the π and σ polarizations. The background of the phonon sideband has been subtracted from the magnon sidebands. For these polarizations we did not find an obvious secondary magnon peak between the exciton and the main magnon peak as the theory predicts. Instead, there exists a high shoulder [Fig. 3(b)]. This is perhaps not surprising in view of the many approximations we have been forced to make. Further, we did not consider the dispersion of the exciton and its linewidth; that is, we neglected the spectral distribution of the exciton. If we took account of these factors, the consistency between experiment and theory would have been improved. In spite of the secondary peak, theory predicts higher transition intensity between the exciton and the magnon peak. This is consistent with the experiment.

However, this secondary magnon peak was observed in the σ'-polarization absorption spectrum, as shown in Fig. 4(a). It is separated from the exciton by 4.2 cm^{-1}, and comes mainly from the term G_1 in Eq. (16). The other terms contribute only a weak shoulder. Here G_1 is related to the electric dipole matrix element between intrachain ions, which have the strongest exchange interaction. On the other hand, according to the analysis of Sec. IV A, when the neighbor ion is in a magnon state with very low energy, it is expected that the resultant odd parity component of the wave function of a Tanabe-Moriya-Sugano ion pair will be larger than when it is in a magnon state with higher energy.

For the σ'-polarization emission contribution from

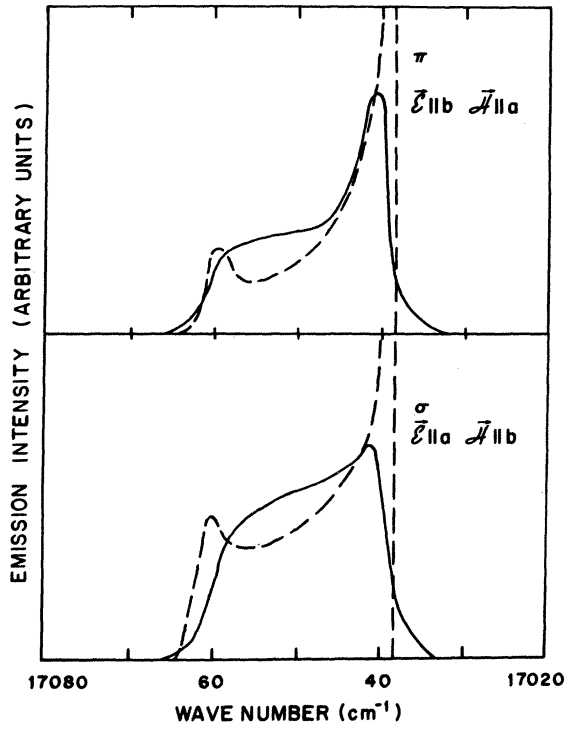

FIG. 10. The observed (solid) and calculated (dashed) line shapes of magnon sidebands for the π- and σ-polarization emission spectra. The background of the phonon sideband has been subtracted from the data of the magnon sideband.

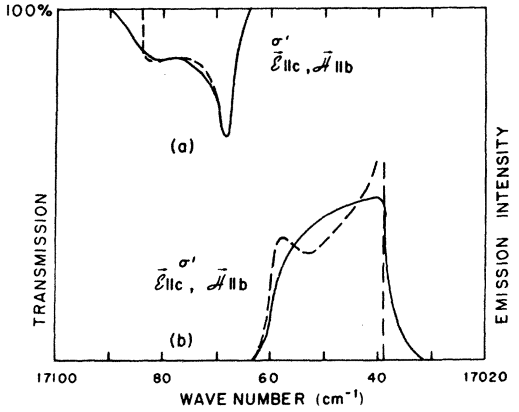

FIG. 11. The observed (solid) and calculated (dashed) line shapes of the magnon sidebands for the σ'-polarization absorption (a) and emission (b) spectra. The background of the phonon sideband has been subtracted from the data of the magnon sideband.

the term G_1 in Eq. (15) produces an increase in strength in the shoulder, but the secondary magnon peak does not appear. The comparison of the theoretical curves with the experimental is presented in Fig. 11 and the agreement again is satisfactory. For the absorption, a parameter $\alpha=0.45$ was adapted [see Eq. (19) below].

As it is well known, in the absorption spectrum, because of the interaction between excitons and magnons, the position of the magnon peak is shifted toward the origin (the exciton position).[13,14] The effect is equivalent to the decrease of the number of the nearest neighbors. Approximately, the magnon dispersion for the absorption spectrum can be modified by replacing the expressions (6) and (8) with

$$A'=g\mu H_a-2S(2-\alpha)(J_1+J_2+J_3)$$
$$+16S(J_4+J_5+J_6) \tag{17}$$

and

$$J_k'=2S(2-\alpha)(J_1\cos\tfrac{1}{2}k_a a+J_2\cos k_b b+J_3\cos\tfrac{1}{2}k_c c)\ . \tag{18}$$

Here

$$\alpha=\frac{J_1S-J_1'S'}{JS}\ , \tag{19}$$

where S' is the effective spin of an excited ion, and J' is the exchange constant between the excited ion and its nearest neighbor at the ground state along the chain a. In quasi-one-dimensional magnetic systems, there are only two nearest neighbors having a strong exchange interaction; therefore, the influence of the interaction between excitons and magnons will be particularly evident. We expect the magnon shoulder in the absorption (excitation) spectrum to be closer to the exciton. From the position of the magnon sideband in absorption in Fig. 3(a) with splitting $\Delta\simeq16$ cm^{-1}, we estimate $\alpha\simeq0.7$. For CMC, $S=\frac{5}{2}$, $S'=\frac{3}{2}$, we find $J'=0.5J$. A similar result has been found in $RbMnF_3$.[11,12] As noted above, for the calculated curve in Fig. 10(a), in order to fit the secondary magnon peak, we adopted $\alpha=0.45$, a smaller value. This is reasonable since J' in Eq. (19) is a function of the magnon energy $E_m(k)$. The smaller the magnon energy, the larger the value of J'. For $E_m(k)\approx0$, $J'\approx J$, so $\alpha\approx0$.

In the π-polarization excitation (absorption) spectrum, there is a shoulder at the low-energy side of the exciton. In the σ- and α-polarization emission spectrum, there are some shoulders at the high-energy side of the exciton. We do not know their origins. One of the possibilities is that the shoulder in excitation spectrum is the excitation of a hot magnon band.[15] At the Brillouin-zone boundary Y, T, and Z, the magnon states have a higher density and very low energy. At the temperature range under consideration, it is possible to have a considerable

thermal population of these magnons. The transition from the hot magnon band will be electric dipole allowed. By the same argument, we can interpret the shoulder of the exciton in the emission as the transition $|E_A\rangle + |M_B\rangle \rightarrow |G_A\rangle + |G_B\rangle$, that is, one exciton at sublattice A and one hot band magnon at sublattice B transit to their ground states simultaneously. This is the inverse process of the sideband absorption and is an anti-Stokes sideband emission which has been observed in the π-polarization luminescence spectrum of MnF_2 at as high temperature as 13.3 K.[12]

D. Dynamic process

The exciton motion in antiferromagnets might be a coherent process on one sublattice or a diffusive process on both sublattice.[16] The former is a zero-magnon process and might be important at low temperatures. The latter is a two-magnon process, that is, the intersublattice transfer of excitons can take place only when two magnons are created and/or annihilated simultaneously, therefore, this process is important only at high temperatures and can be neglected at low temperatures. In one-dimensional antiferromagnets, because of the very weak intrasublattice exchange interaction, the intrasublattice coherent transfer of the excitons is negligible. As a result, at low temperatures, the energy migration would be very slow, i.e., the excitons are very localized. The localization of the excitation makes the trapping probability of excitons very low.[1–3] The decay process of exciton, measured in CMC, is typically exponential at 1.8 K (Fig. 6). This indicates that there is no biexcitonic annihilation as in MnF_2,[17] and also no process of diffusion-limited energy transfer. It seems that the energy decay of the excited ion is confined within the ion itself. But for the localization model, the lifetime of 0.57 ms of the exciton seems too short. $^4T_1$ states in Mn^{2+} normally should have lifetimes of 1–10 ms. It is likely that a multiphonon nonradiative decay process involving the hydrogen-water vibrations relaxes the exciton quite rapidly.

Unlike three-dimensional antiferromagnets, in CMC, there exists short-range ordered chains in a wide temperature range above T_N. At $T = 3T_N$, independent chains of about five correlated spins may exist.[6] Thus it is expected that some sharp excitation can be observed above T_N. This was verified by our optical measurement. At $T > T_N$, we still observed the exciton and magnon lines (Fig. 5). It would be very interesting to study the dynamic process of the exciton and the magnon behavior in the short-range ordered region. Unfortunately, above T_N, the signals are complicated by overlap with the phonon sideband which become stronger as the temperature is increased.

V. CONCLUSIONS

The no-phonon, no-magnon exciton lines in absorption, excitation, and emission spectra have been observed for the first time in a one-dimensional magnetic system. The exciton transition is electric dipole allowed. The magnon sideband in emission is a single-ion transition and both electric and magnetic dipole allowed. However, the magnon sideband in absorption is an ion pair process and the electric dipole activation is weakened. As a result, this process gives rise to only a weak shoulder. An exception is the secondary magnon peak with very low energy, which comes from the intrachain ion pairs with the strongest interaction and has a stronger electric dipole activation. Quasi-one-dimensional magnetic interaction produces the peculiar line shapes of the magnon sideband observed experimentally. The exponential decay process at 1.8 K is one evidence for the localization of the exciton in the one-dimensional antiferromagnetic system. In order convincingly to prove the localization characteristics, more work needs to be done. On the other hand, the short lifetime and the weak intensity of the exciton should be studied in more detail.

We are grateful to Professor D. L. Huber, Dr. R. M. Macfarlane, Professor D. S. McClure, and Dr. R. M. White for helpful discussions. One of the authors expresses his thanks to Dr. D. Pearson for providing equipment for growing the crystals, to Mr. M. Broer, C. Levey, and J. Pellegrino for help with experimental techniques, to Mr. Lou Liren and Huang Shihua, and Dr. Shui Lai for their miscellaneous assistance. This work was supported by the NSF under Grant No. DMR-79-20070 and by NATO under Grant No. RG-1456.

APPENDIX A

The symmetric operations of the magnetic space group $P_{_{2bc'ca'}}$ (see Fig. 1): (i) $(E|0)$, the identity operator; (ii) $(C_2^b|0)$, rotation about b by 180°; (iii) $(C_2^{C_B}|0)$, rotation about C_B by 180°; (iv) $(C_2^{C_A}|T)$, rotation about C_A by 180°, followed by time inversion; (v) $(C_2^a|\pm a/2)$, rotation about a by 180°, followed by translation $\pm a/2$; (vi) $(I_M|T)$, inversion about M, followed by time inversion; (vii) $(I_N|0)$, inversion about N; and (viii) $(T|\pm b)$, time inversion, followed by translation $\pm b$.

*Permanent address: Institute of Physics, Chinese Academy of Science, Beijing, Peoples Republic of China.
†Present address: FB Physik, Universität, 2900 Oldenburg, Federal Republic of Germany.

[1]H. Yamamoto, D. S. McClure, C. Marzzacco, and M. Waldman, Chem. Phys. 22, 79 (1977).
[2]G. L. McPherson and A. H. Francis, Phys. Rev. Lett. 41, 1681 (1978).
[3]R. Ya-Bron, V. V. Eremenko, and E. V. Matyushkin, Sov. J. Low Temp. Phys. 5, 314 (1979).
[4]S. J. Jensen and P. Andersen, Acta Chem. Scand. 16, 1890 (1962).
[5]R. D. Spence, W. J. M. de Jonge, and V. V. S. Rama Rao, J. Chem. Phys. 51, 4694 (1969).
[6]J. Skalyo, Jr., G. Shirane, S. A. Friedberg, and H. Kobayashi, Phys. Rev. B 2, 4632 (1970).
[7]D. D. Sell, R. L. Greene, and R. M. White, Phys. Rev. 158, 489 (1967).
[8]Y. Tanabe, T. Moriya, and S. Sugano, Phys. Rev. Lett. 15, 1023 (1965).
[9]R. Loudon, Adv. Phys. 17, 243 (1968).
[10]R. L. Greene, D. D. Sell, R. S. Feigelson, G. F. Imbusch, and H. J. Guggenheim, Phys. Rev. 171, 600 (1968).
[11]R. E. Dietz and A. Misetich, *Localized Excitations in Solids* (Plenum, New York, 1968), p. 366.
[12]T. C. Chiang, P. R. Solvi, J. Davies, and Y. R. Shen, Solid State Commun. 26, 217 (1978).
[13]J. B. Parkinson and R. Loudon, J. Phys. C 1, 1568 (1968).
[14]R. J. Elliot, M. F. Thorpe, G. F. Imbusch, R. Loudon, and J. B. Parkinson, Phys. Rev Lett. 21, 137 (1968).
[15]R. S. Meltzer, M. Lowe, and D. S. McClure, Phys. Rev. 180, 561 (1969).
[16]K. Ueda and Y. Tanabe, J. Phys. Soc. Jpn. 48, 1137 (1980).
[17]B. A. Wilson, J. Hegarty, and W. M. Yen, Phys. Rev. Lett. 41, 268 (1978).